

1 **Textural properties of synthetic nano-calcite produced by** 2 **hydrothermal carbonation of calcium hydroxide**

3
4 G. Montes-Hernandez ^{*a}, A. Fernández-Martínez ^{a,b}, L. Charlet ^a, D. Tisserand ^a, F. Renard ^{c,d}

5
6 ^a LGIT, University of Grenoble and CNRS, BP 53 X, 38420 Grenoble Cedex 9

7 ^b Institut Laue-Langevin, B.P. 156, 38042 Grenoble Cedex 9

8 ^c Physics of Geological Processes, University of Oslo, Norway

9 ^d LGCA, University of Grenoble and CNRS, BP 53 X, 38420 Grenoble Cedex 9

10
11 ^{*} Corresponding author: German Montes-Hernandez

12 E-mail address: German.MONTES-HERNANDEZ@obs.ujf-grenoble.fr

13 german_montes@hotmail.com

1 **Abstract**

2

3 The hydrothermal carbonation of calcium hydroxide (Ca(OH)_2) at high pressure of CO_2
4 (initial $P_{\text{CO}_2} = 55$ bar) and moderate to high temperature (30 and 90°C) was used to synthesize
5 fine particles of calcite. This method allows a high carbonation efficiency (about 95% of
6 Ca(OH)_2 - CaCO_3 conversion), a significant production rate ($48 \text{ kg/m}^3\text{h}$) and high purity of
7 product (about 96%). However, the various initial physicochemical conditions have a strong
8 influence on the crystal size and surface area of the synthesized calcite crystals. The present
9 study is focused on the estimation of the textural properties of synthesized calcite
10 (morphology, specific surface area, average particle size, particle size distribution and particle
11 size evolution with reaction time,) using Rietveld refinements of X-ray diffraction spectra,
12 BET measurements and, scanning and transmission electron microscope (SEM and TEM)
13 observations. This study demonstrate that the pressure, the temperature and the dissolved
14 quantity of CO_2 have significant effect on the average particle size, specific surface area,
15 initial rate of precipitation, and on the morphology of calcium carbonate crystals. In contrast,
16 these PTx conditions used herein have insignificant effect on the carbonation efficiency of
17 Ca(OH)_2 .

18 Finally, the results presented here demonstrate that nano-calcite crystals with high specific
19 surface area ($S_{\text{BET}}=6-10 \text{ m}^2/\text{g}$) can be produced, with a high potential for industrial
20 applications such as adsorbents and/or filler in papermaking industry.

21

22

23 **Keywords:** A1. Crystal morphology; A1. X-ray diffraction; A2. Hydrothermal crystal
24 growth; B1. Nanomaterials; B1. Minerals

25

1 **1. Introduction**

2 Calcium carbonate is an inorganic compound that has been widely studied due to its
3 abundance in nature as a mineral and biomineral. Calcium carbonate particles have three
4 crystal morphologies and structures, which are generally classified as rhombic calcite, needle-
5 like aragonite and spherical vaterite. Calcite belonging to Trigonal-Hexagonal-Scaleno-hedral
6 Class is the most stable phase at room temperature under normal atmospheric conditions,
7 while aragonite and vaterite belong to Orthorombic-Dipyramidal Class and Hexagonal-
8 Dihexagonal Dipyramidal Class, respectively. The later are metastable polymorphs which
9 readily transform into the stable calcite. The specific formation of one of the polymorphs of
10 crystalline calcium carbonate particles depends mainly on the precipitation conditions, such as
11 pH, temperature and supersaturation. Supersaturation is usually considered to be the main
12 controlling factor [1]. Many experimental studies have been reported about the synthetic
13 precipitation of the various forms of calcium carbonate and the conditions under which these
14 may be produced, including the importance of initial supersaturation, temperature, pH and
15 hydrodynamics. The effect of impurities and additives has also been well studied [see for ex.
16 2-15].

17 Limestone is the most common natural form of calcium carbonate. It has extensive industrial
18 applications: it is one of the components of cements and several construction materials.
19 However, the actual usefulness of calcium carbonate extends far beyond the current usages to
20 which limestone is put. For instance, fine calcium carbonate particles are an active ingredient
21 in commercially available antacid tablets. The calcite is also efficient filler in printing inks
22 and papermaking industry [16].

23 The most commonly used industrial process for obtaining CaCO_3 powder involves the
24 following steps: (a) the production of quicklime (CaO) and carbon dioxide by calcinations of
25 limestone; (b) the transformation of quicklime to slaked lime slurry (a suspension of Ca(OH)_2)

1 particles) by controlled addition of water; and finally (c) the carbonation reaction (Eq. 1), in
 2 which the CO_2 is bubbled through an aqueous slurry of slaked lime [17].



4 The carbonation reaction is the crucial step determining the textural properties (such as
 5 average particle size, particle size distribution, morphology and specific surface area) of the
 6 obtained product. For example, the morphology of the precipitated calcite, at typical
 7 temperatures of industrial process (between 30 and 70 °C), is normally the scalenohedral one
 8 bounded by the $\{21\bar{1}\}$ form. Synthetic scalenohedral calcite is generally produced through a
 9 batch carbonation method. The rhombohedral morphology, bounded by the $\{104\}$ form, is
 10 usually precipitated by using solution routes, but rarely by the mentioned industrial process.
 11 The carbonation of $\text{Ca}(\text{OH})_2$ suspension without the addition of additives allows to control the
 12 textural properties of calcite precipitates [17, 18-19]. Therefore, the development of new
 13 industrial carbonation routes for the production of calcite with different textural properties in
 14 the absence of expensive additives is of great interest. The industrial applications of CaCO_3
 15 are mainly determined by the textural properties, such as average particle size, particle size
 16 distribution, morphology, specific surface area and/or polymorphism [17].

17 Recently, the hydrothermal carbonation of $\text{Ca}(\text{OH})_2$ suspension in presence of compressed or
 18 supercritical CO_2 was proposed as a novel method to produce powdered calcite with potential
 19 interest to industrial applications [17, 20]. Then, in the current investigation, the carbonation
 20 of calcium hydroxide suspension at high pressure of CO_2 (initial $P_{\text{CO}_2} = 55$ bar) and moderate
 21 to high temperature (30 and 90°C) was used to synthesize fine particles of calcite. In a
 22 previous study it was shown that the proposed method allowed a high carbonation efficiency
 23 (about 95% of $\text{Ca}(\text{OH})_2$ - CaCO_3 conversion), a significant production rate (48 kg/m³h) and
 24 high purity of product (about 96%) [21]. In this study, it was also observed that the
 25 carbonation efficiency was not significantly affected by Pressure and Temperature (P-T)

1 conditions after 24 h of reaction. This confirmed the low reactivity of molecular CO₂ on
2 calcite dissolution [22] and precipitation [21]. In contrast, the initial rate of calcite
3 precipitation was proportional to dissolved CO₂. For this case, it increased from 4.3 mol/h in
4 the “90 bar – 90 °C” system to 15.9 mol/h in the “55 bar – 30 °C” system. This kinetic
5 behaviour should have a direct influence on the texture properties, particularly on the average
6 particle size, particle size distribution, specific surface area and crystal morphology. For this
7 reason, the aim in the present study is mainly focused on the quantification of the textural
8 properties of synthesized calcite by using Rietveld refinement of X-ray diffraction (XRD)
9 spectra, Brunauer-Emmet-Teller (BET) specific surface area measurements and Scanning and
10 Transmission Electron Microscope (SEM and TEM) observations. By varying the initial P, T,
11 and molar fraction for calcite synthesis, different grain sizes could be produced. For this
12 study, nanoparticles are defined as those characterized by 2 to 3 dimensions lower than 300
13 nm.

15 **2. Materials and methods**

16 *2.1 Synthesis of calcite (stirred reactor)*

17 One litre of high-purity water with electrical resistivity of 18.2 MΩ·cm and 74.1 g of
18 commercial calcium hydroxide (provided by Sigma-Aldrich) with 96% chemical purity (3%
19 CaCO₃ and 1% other impurities) were placed in a titanium reactor (autoclave with internal
20 volume of two litres). The hydroxide particles were immediately dispersed with mechanical
21 agitation (400 rpm). The dispersion was then heated to 90°C with a heating system adapted to
22 the reactor. When the dispersion temperature was reached, 80.18 g of CO₂ (provided by Linde
23 Gas S.A.) were injected in the reactor and the total pressure in the system was immediately
24 adjusted to 90 bar by argon injection (see Figure 1a). Under these P-T conditions, the vapour
25 phase consists mainly of an Ar + CO₂ mixture with the CO₂ in a supercritical state (Figure

1 1b). In order to evaluate the precipitation (or production) rate, five different reaction times
2 were considered (0.25, 0.5, 4, 15 and 24 h). The experiments were also carried out at 30°C
3 and 55 bar for reaction durations of 0.25, 4 and 24 h. For this second case, 96.05 g of CO₂
4 were initially injected in the reactor. At 55 bar and 30°C, the vapour phase consists mainly of
5 gaseous CO₂ (Figure 1b). A complete description on the experiments was reported by
6 Montes-Hernandez et al. [21].

7 Additionally, a semi-batch system (sampling with time) was performed in order to measure
8 the pH (using MA235 pH/ion analyzer) and calcium concentration (using ICP Perkin Elmer
9 Optima 3300 DV) in filtered solutions. For this case, about 25 ml of suspension were sampled
10 in the reactor as a function of time (0, 2, 6, 10 and 30 minutes) during calcite precipitation.
11 The P-T conditions were the same above cited, but, only 3g of calcium hydroxide were placed
12 in the reactor. This allows better particle dispersion and a faster dissolution of calcium
13 hydroxide. In addition, for these experiments, approximately 14.5 g of CO₂ were injected in
14 the system. Note that the pH and Ca-concentration measurements were carried out at 25 °C
15 after filtration, cooling and degasification of the solutions.

16 *2.2 Characterization of the solid particles size and specific surface area*

17 Morphological analyses of the solid products were performed by Scanning Electron
18 Microscopy (SEM), with a HITACHI S-4800 microscope. Isolated fine particles (oriented on
19 carbon Ni grids) of the starting material and products were also studied using a JEOL 3010
20 Transmission Electron Microscope (TEM) equipped with an energy dispersive X-ray analyser
21 (EDS) to image the morphology of the particles and to identify the precipitated phases.

22 The specific surface area of powdered calcite (four samples) was estimated by applying the
23 Brunauer-Emmet-Teller (BET) equation and by using 16.3 Å² for cross-sectional area of
24 molecular N₂. The N₂ adsorption experiments were performed using a Micrometrics ASAP
25 2010 system.

1 2.3 X-ray diffraction analysis of the solid phase

2 X-Ray Powder Diffraction (XRD) analyses were performed using a Kristalloflex 810,
3 SIEMENS diffractometer in Bragg-Brentano geometry. The XRD patterns were collected
4 using Co $k\alpha_1$ ($\lambda_{k\alpha_1}=1.7889 \text{ \AA}$) and $k\alpha_2$ ($\lambda_{k\alpha_2}=1.7928 \text{ \AA}$) radiation in the range $2\theta = 5 - 80^\circ$
5 with a step size of 0.02° and a counting time of 8 seconds per step.

6 The widths of the diffraction peaks in a diffraction pattern are mainly affected by two
7 contributions: (1) the instrumental resolution and (2) microstructural effects related to the size
8 of the crystallites or to the strains within their crystal structure. Both effects are convoluted in
9 a diffraction pattern but can be separated by the use of convolution or deconvolution methods.

10 A convolution method (Rietveld refinement) has been used in this study to account for size
11 and strain effects. For this purpose, an X-ray diffraction pattern of a microstructure-free
12 sample (SiO_2 in our case) has been measured, in order to isolate the instrumental resolution
13 effect. In this way, further Rietveld refinements of the samples using size and strain models
14 account only for microstructural effects.

15 In order to get a more detailed knowledge on the texture of the calcite particles, we have
16 performed microstructural analyses within the Rietveld refinement of the X-ray diffraction
17 data. The method is sensitive to the anisotropy of the crystallites, as a refinement of the full
18 X-ray pattern is performed, which includes reflections of different reciprocal space directions.

19 In addition, the combination of this crystallographic approach with the use of adsorption-
20 based methods for the calculation of specific surfaces gives an idea of the crystallinity and
21 aggregation state of the samples, as different entities are probed: the
22 aggregation/agglomeration of different crystalline grains can decrease the porosity and thus
23 prevent the access of the N_2 molecules to the entire surface, while the X-ray diffraction probes
24 the coherent domains of the sample and yields and estimation of its crystallinity.

1 Rietveld refinement of the powder diffraction patterns has been carried out using the FullProf
2 package (Windows version, February 2007) [23]. The pseudo-Voigt profile function of
3 Thompson, Cox and Hastings [24] was used to fit the peak shapes. The parameters
4 constituting the angular-dependent microabsorption correction were refined for each sample.
5 Multiphase analysis was performed introducing a portlandite phase (calcium hydroxide) in the
6 samples when the portlandite to calcite phase transition was not completely accomplished.
7 Structural refinements of calcite were performed considering the R-3C space group and taking
8 as initial values those obtained in the x-ray powder diffraction study reported by Maslen et al.
9 [25]. Scale factor, zero point, cell dimensions, atomic coordinates and Debye Waller factors
10 were refined. Background was refined by adjusting a fourth order polynomial. The
11 instrumental contribution to peak broadening was determined with a SiO₂ sample [26]. The
12 asymmetry parameters of the L. Finger correction S_L and S_D [27], and the Cagliotti
13 parameters [28] were refined for the standard sample of SiO₂ and kept fixed during the
14 refinements of the calcite patterns. Anisotropic size broadening was modeled in terms of
15 spherical harmonics and the coherent domain average apparent size along each reciprocal
16 lattice vector was calculated. Coherent domain average size was calculated averaging the
17 resulting size of each of the reciprocal space distances measured. Volume and specific surface
18 area of the coherent domains were calculated by assuming rectangular prisms with edges
19 along the reciprocal space [100], [010] and [001] directions. The Cagliotti parameter U was
20 refined in order to account for some isotropic strain in the Gaussian component of the peak
21 profile. The strain is given in %%: a strain of x %% means a strain ratio of $\varepsilon = (d_i - d_f) / d_i \times 10000$,
22 being d_i and d_f the strain-free crystallite size and the strained crystallite size respectively. Errors in size
23 and strain have been estimated by performing refinements with different starting points, thus probing
24 the stability of the result. Errors in size and strain are better than 10%.

25

26

1
2
3
4
5
6
7
8
9
10
11
12
13
14
15
16
17
18
19
20
21
22
23

3. Results and discussion

3.1. Reaction mechanism of calcite precipitation

The aqueous carbonation of Ca(OH)_2 described by the global reaction (1) is an exothermic process that concerns simultaneously the dissolution of Ca(OH)_2 ,



and the dissociation of aqueous CO_2 ,



these processes produce a fast supersaturation (S_I) of solution with respect to calcite,

$$S_I = \frac{(\text{Ca}^{2+})(\text{CO}_3^{2-})}{K_{sp}} > 1 \quad (4)$$

where (Ca^{2+}) and (CO_3^{2-}) are the activities of calcium and carbonate ions in the solution, respectively, and K_{sp} is the thermodynamic solubility product of calcite. Then, the nucleation stage (formation of nuclei or critical cluster) takes place in the system (see Fig. 2),



Finally, the crystal growth occurs spontaneously until the equilibrium calcite and the solution is reached (see for ex. Fig. 3),



The metastable crystalline phases of CaCO_3 , such as vaterite and aragonite, were not identified in the X-ray diffraction spectra during the Ca(OH)_2 carbonation process in our experiments. A small quantity of crystalline aragonite can be precipitated when the reactor is depressurized after the water-cooling stage (for more details, see [21]).

1
2
3
4
5
6
7
8
9
10
11
12
13
14
15
16
17
18
19
20
21
22
23
24
25

3.2. Microscopic and BET measurements

For this study, the presence of supercritical CO₂ did not have a clear effect on the Ca(OH)₂ carbonation process. In contrast, the P-T conditions had a significant effect on carbonation rate [21]. In fact, the precipitation rate is proportional to the quantity of dissolved CO₂. This justifies a higher rate of calcite precipitation at lower temperature. Consequently, we propose that the precipitation rate for these systems is linked to the particle size and calcite-crystal morphology. At higher precipitation rate (15.9 mol/h), i.e. for the "55 bar – 30 °C" system, the TEM micrographs showed scalenohedral calcite as dominant morphology (Figure 4b). For this case, sub-micrometric isolated particles (< 1 µm) and micrometric aggregates and/or agglomerates (< 5 µm) of calcite were observed after 24 h of reaction. A slight proportion of rhombohedral calcite was also observed (Figure 4b). The BET measurements reveal a high specific surface area (9.7 m²/g) compared with typical values of powdered calcite. This value leads to a sub-micrometric average particle size of 0.22 µm assuming spherical or cubic geometry. Obviously, the specific surface area and average particle size of solid matrix depend on the reaction time before equilibrium system (this will be described in the following sub-section). In contrast, at high pressure and temperature, i.e. for the "90 bar – 90 °C" system (precipitation rate = 4.3 mol/h), the TEM micrographs showed rhombohedral calcite as dominant morphology in the product. In this case sub-micrometric isolated particles (< 1 µm) and micrometric agglomerates (< 5 µm) of calcite were observed after 24 h of reaction (Figure 4a). For this case, the specific BET surface area and average particle size were 6 m²/g and 0.36 µm, respectively.

1
2
3
4
5
6
7
8
9
10
11
12
13
14
15
16
17
18
19
20
21
22
23
24
25

3.3. Rietveld refinements

The results of the Rietveld refinements are shown in Table 1 and the observed and calculated powder diffraction spectra of 2 different samples are presented in Figure 5. Plots of the evolution of the coherent domain average size, maximum and minimum coherent domain size and specific surface area for the calcite samples synthesized under 90 bar of total pressure and 90 °C are presented in Figure 2 for a better interpretation of the results. A residual phase of Portlandite was found in all the refinements up to 4 hours of reaction time; from that reaction time only the calcite phase is present. The growth of the coherent domain size of samples synthesized at $P_{\text{total}} = 90$ bar follows a quick evolution during the first 5 hours of the reaction.

3.4. Process of calcite growth

The increase in coherent domain size as detected by X-ray diffraction is accompanied by a precipitation-dissolution process of the crystallites in their very early stage of nucleation (first 0.5 h). This fact can be clearly observed following the kinetics of growing of the crystallites from the XRD coherent domain size shown in Figure 6: it reflects a continuous growing of the minimum size of the coherent domains, while the maximum size decreases from 168 nm to 137 nm when passing from 0.25 h to 0.5 h of reaction. This behaviour is observed later in the reaction: the maximum size of the coherent domains decrease from 412 nm after 15 h of reaction to 337 nm after 24h. This decrease can be interpreted in terms of a dissolution process of the coherent domains, given that there is an excess of CO_2 concentration in the reactor leading to an acidic condition which would explain this behaviour. Note that we cannot confirm the same behaviour occurring in the samples synthesized at 50 bar of P_{CO_2} and 30 °C as we only extracted samples at 0.25 h and 24 h of reaction.

1 The experimental BET specific surface area and the calculated average coherent domain
2 surface area resulting from the Rietveld refinements for each sample and experimental
3 synthesis conditions are presented in Table 2. The TEM micrographs in Figure 4 show a well
4 crystallized rhombohedral calcite with BET calculated average sizes in the order of 0.36 μm .
5 The BET calculated average size is obtained by assuming cubic particle shape. The values for
6 the BET and XRD specific surface areas differ by a factor of ~ 5 for the samples of the “50 bar
7 – 30 $^{\circ}\text{C}$ ” synthesis and a factor of ~ 3 for the “90 bar – 90 $^{\circ}\text{C}$ ” synthesis. The values obtained
8 from XRD are always higher than the BET, as expected from the values for the crystallites
9 sizes. The fact that the proportionality factor between BET and XRD goes from 5 to 3 can be
10 interpreted in terms of aggregation state: the coherent domains are less aggregated when the
11 synthesis is done at higher pressure and temperature. TEM observations, even though not
12 giving a statistical mean of the ensemble, reveal crystallite sizes on the same order as the
13 obtained by XRD. These two facts have direct implications on the colloidal behaviour of the
14 calcite as well as in its behaviour with respect to solubility and dissolution processes.

15

16 **4. Conclusion**

17 This study demonstrate that the Pressure, the temperature and the dissolved quantity of CO_2
18 have significant effect on the average particle size, specific surface area, initial rate of
19 precipitation, and on the morphology of calcium carbonate crystals. In contrast, these PTx
20 conditions used herein have insignificant effect on the carbonation efficiency of $\text{Ca}(\text{OH})_2$. In
21 addition, molecular CO_2 (in gaseous or supercritical state) seems also to have an insignificant
22 effect on the calcite precipitation.

23 Rietveld analyses of the XRD patterns yield information on the growth behaviour and the
24 crystallinity of the samples. While nanoparticles are obtained at 55 bar and 30 $^{\circ}\text{C}$, the sub-
25 micrometric well defined crystals are obtained at 90 bar and 90 $^{\circ}\text{C}$. First, a dissolution-

1 precipitation process is observed in the first stages (first hour) of the synthesis. Second, the
2 ratio between the XRD and BET specific surface areas decreases from 5 to 3 when changing
3 the initial thermodynamic conditions from 50 bar and 30 °C to 90 bar and 90 °C. This
4 demonstrates that better crystallized samples are obtained when raising the temperature and
5 pressure conditions, and a higher degree of aggregation of the crystallites in the 50 bar and 30
6 °C samples. These analyses give useful information on the microstructural characteristics of
7 the calcite samples obtained from hydrothermal conditions.

8 The results presented here demonstrate that nano-calcite crystals, with high specific surface
9 area can be produced, with a high potential for industrial applications such as adsorbents
10 and/or filler in papermaking industry.

11
12
13
14
15
16
17
18
19
20
21
22
23
24
25

1
2
3
4
5
6
7
8
9
10
11
12
13
14
15
16
17
18
19
20
21
22
23
24
25

Acknowledgements

The authors are grateful to the National Research Agency, ANR (GeoCarbone-CARBONATATION project) and the National Research Council (CNRS), France, for providing a financial support for this work. This study has also been financed through collaboration between the University of Grenoble (German Montes-Hernandez, François Renard) and Gaz de France (Christophe Rigollet, Samuel Saysset, Rémi Dreux). The authors are grateful to S. Petit who allowed the BET measurements to be performed in her laboratory. Nicolas Geoffroy is acknowledged for his help during the XRD experiments.

1
2
3
4
5
6
7
8
9
10
11
12
13
14
15
16
17
18
19
20
21
22
23
24
25

References

- [1] Y. S. Han, G. Hadiko, M. Fuji, M. Takahashi, *J. Crystal Growth* 276 (2005) 541.
- [2] L. Moore, J. D. Hopwood, R. J. Davey, *J. Crystal Growth* 261 (2004) 93.
- [3] K. J. Westin, A. C. Rasmuson, *J. Colloids Interface Sci.* 282 (2005) 370.
- [4] H. Tsuno, H. Kagi, T. Akagi, *Bull. Chem. Soc. Jpn.* 74 (2001) 479.
- [5] Y. Fujita, G. D. Redden, J. Ingram, M. M. Cortez, G. Ferris, R. W. Smith, *Geochem. Cosmochem. A.* 68 (2004) 3261.
- [6] S. J. Freij, A. Godelitsas, A. Putnis, *J. Crystal Growth* 273 (2005) 535.
- [7] L. A. Gower, D. A. Tirrell, *J. Crystal Growth* 191 (1998) 153.
- [8] R. G. Jonasson, K. Rispler, B. Wiwchar, W. D. Gunter, *Chem. Geol.* 132 (1996) 215.
- [9] A. Chrissanthopoulos, N. P. Tzanetos, A. K. Andreopoulou, J. Kallitsis, E. Dalas, *J. Crystal Growth* 280 (2005) 594.
- [10] M. Menadakis, G. Maroulis, P. G. Koutsoukos, *Computational Materials Science* 38 (2007) 522.
- [11] E. Dousi, J. Kallitsis, A. Chrissanthopoulos, A. H. Mangood, E. Dalas, *J. Crystal Growth* 253 (2003) 496.
- [12] L. Pastero, E. Costa, B. Alessandria, M. Rubbo, D. Aquilano, *J. Crystal Growth* 247 (2003) 472.
- [13] Y. J. Lee, R. Reeder, *Geochem. Cosmochem. A.* 70 (2006) 2253.
- [14] M. Temmam, J. Paquette, H. Vali, *Geochem. Cosmochem. A.* 64 (2000) 2417.
- [15] E. Dalas, A. Chalias, D. Gatos, K. Barlos, *J. Colloids Interface Sci.* 300 (2006), 536.
- [16] Hyun Sook Lee, Tai Hwan Ha, Kwan Kim, *Mater. Chem. Phys.* 93 (2005) 376.

- 1 [17] C. Domingo, J. García-Carmona, E. Loste, A. Fanovich, J. Fraile, J. Gómez-Morales, J.
2 Crystal Growth 271 (2004) 268.
- 3 [18] J. García-Carmona, J. Gómez Morales, R. Rodríguez Clemente, J. Crystal Growth 249
4 (2003) 561.
- 5 [19] J. García-Carmona, J. Gómez Morales, R. Rodríguez Clemente, J. Colloid Interface Sci.
6 261 (2003) 434.
- 7 [20] C. Domingo, E. Loste, J. Gómez-Morales, J. García-Carmona, J. Fraile, J. Supercrit.
8 Fluids 36 (2006) 202.
- 9 [21] G. Montes-Hernandez, F. Renard, N. Geoffroy, L. Charlet, J. Pironon, J. Crystal Growth
10 308 (2007) 228.
- 11 [22] O. S. Pokrovsky, S. V. Gobulev, J. Schott, Chem. Geol. 217 (2005) 239.
- 12 [23] J. Rodríguez-Carvajal, Collected Abstracts of Powder Diffraction Meeting. Ed. by J.
13 Galy. Toulouse, France. 1990.
- 14 [24] P. Thompson, D. E. Cox, J. B. Hastings, J. Appl. Crys. 20 (1987) 79.
- 15 [25] E. N. Maslen, V. A. Streltsov, N. R. Streltsova, Acta Crys. B. 49 (1993) 636.
- 16 [26] Reference n° 00-046-1045 from JCPDS, International Centre for Diffraction Data.
- 17 [27] Finger, L. W., Cox, D. E., Jephcoat, A. P. J. Appl. Crys. 27 (1994) 892.
- 18 [28] Cagliotti, G, Paoletti, A., Ricci, F. P. Nucl. Instr. Meth. 3 (1958) 223.
- 19

1 **Table 1.** Results of the Rietveld refinement of powder diffraction data: average crystallite size, strain,
 2 maximum and minimum average sizes per crystallite and their reciprocal space directions. The error
 3 for all the magnitudes is better than 10%.

P_T (bar)	Reaction time (h)	XRD coherent domain average size (nm)	XRD coherent domain average strain (%)	XRD coherent domain maximum size (nm)	$[h\ k\ l]$ maximum size	XRD coherent domain minimum size (nm)	$[h\ k\ l]$ minimum size	χ^2
55	0.25	42	14	54	[2 0 2]	35	[0 1 2]	10.8
	24	64	14	96	[2 0 2]	38	[0 0 6]	12.7
90	0.25	112	15	168	[2 0 2]	75	[0 1 2]	8.89
	0.5	99	16	137	[1 0 4]	76	[0 1 2]	9.86
	4	157	17	230	[3 0 0]	89	[0 1 8]	18.2
	15	157	14	412	[0 0 6]	92	[0 1 8]	19.6
	24	185	16	337	[2 0 2]	109	[0 1 2]	14.8

5

6

7 **Table 2.** Calculated XRD coherent domain specific surface area and experimental BET specific
 8 surface area. The BET measurements were performed on 4 out of the 7 available samples.

P_T (bar)	Reaction time (h)	XRD coherent domain specific surface (m^2/g)	BET crystallite specific surface (m^2/g)
55	0.25	61.3	14.55
	24	42.7	9.72
90	0.25	24.8	7.06
	0.5	27.9	-
	4	12.6	-
	15	14.4	-
	24	15.3	5.95

9

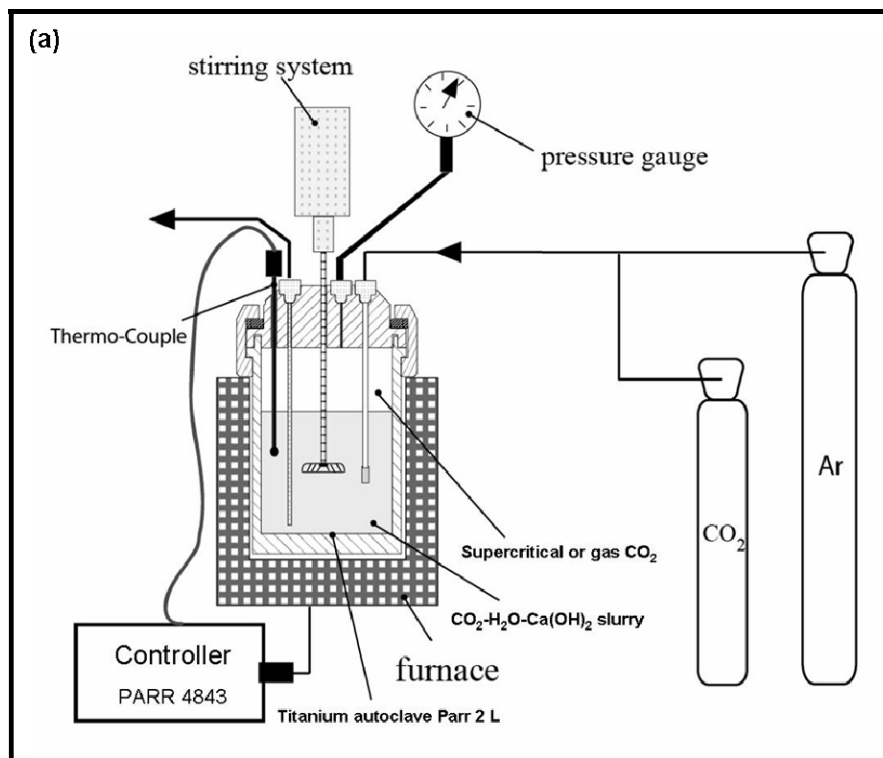
10

11

12

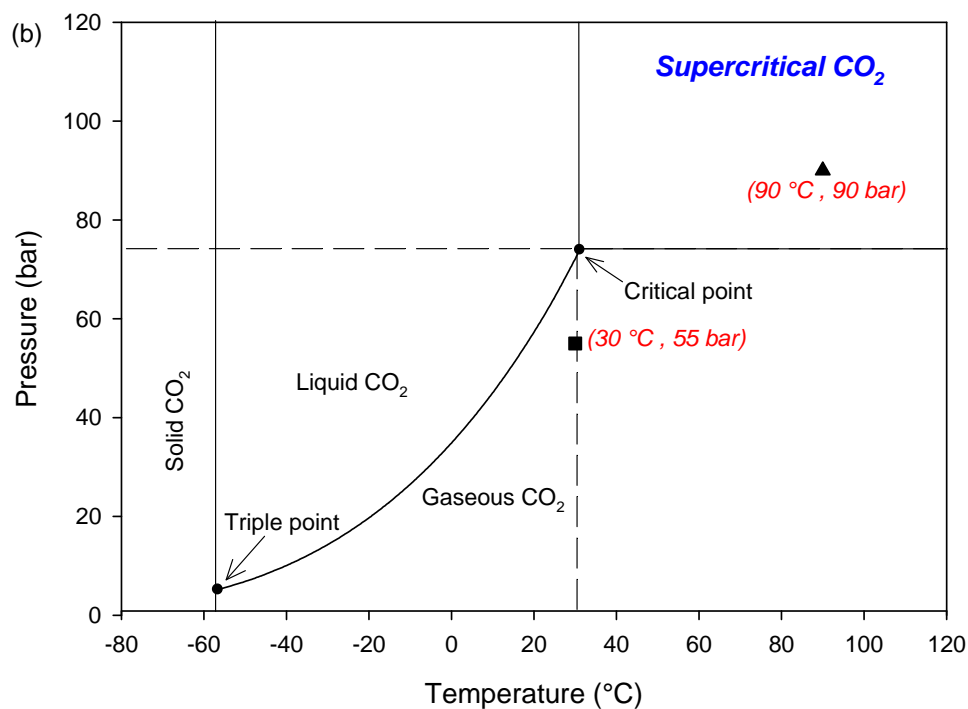
13

14



1

2

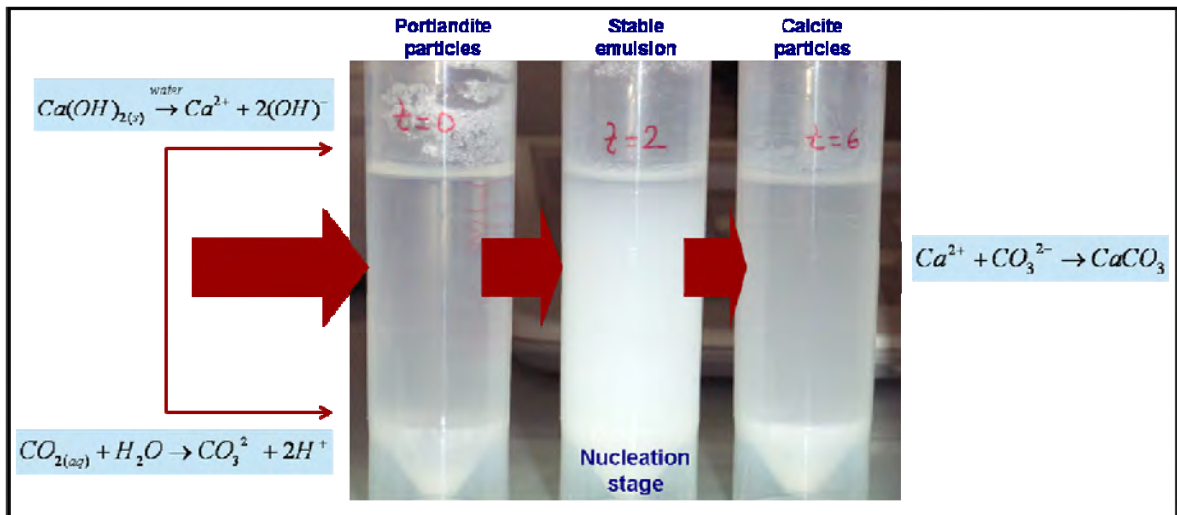


3

4 **Figure 1.** (a) Schematic experimental system for calcite precipitation from CO₂-H₂O-

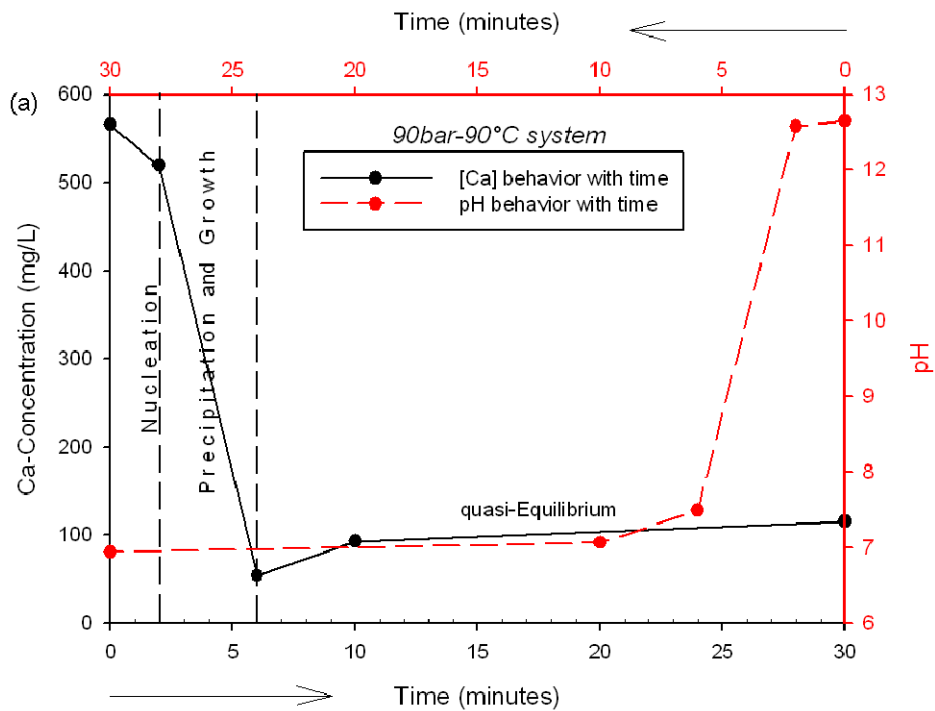
5 Ca(OH)₂ slurry in presence of supercritical and gaseous CO₂ (isobaric system). (b)

6 Experimental conditions represented on a pressure-temperature phase diagram for CO₂.



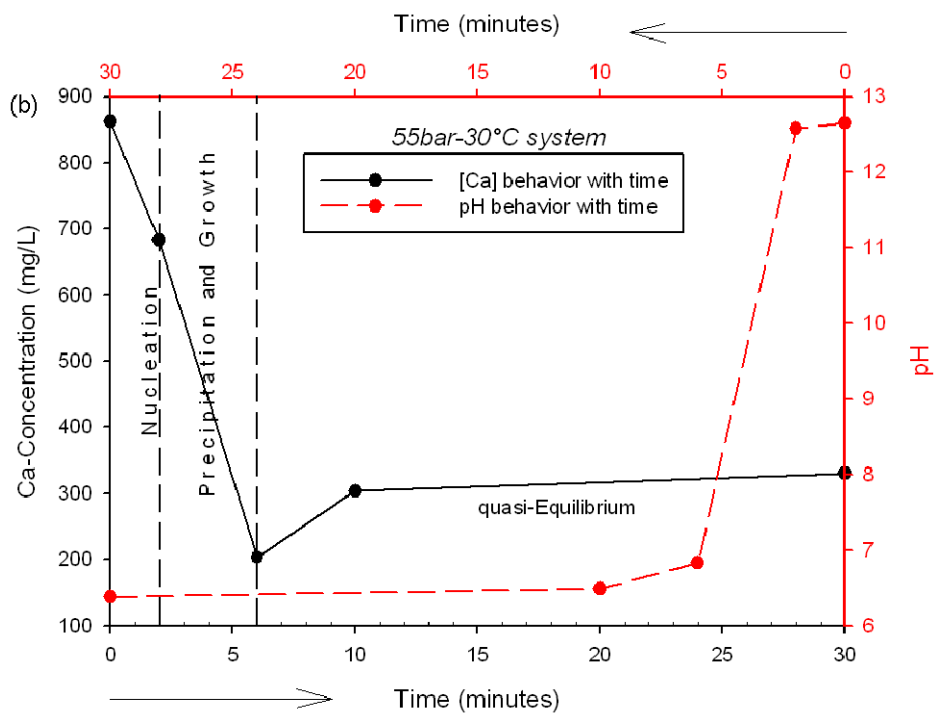
1
2
3
4
5
6
7
8
9
10
11
12
13
14
15
16
17
18
19

Figure 2. Schematic reaction mechanism of calcite precipitation from CO₂-H₂O-Ca(OH)₂ slurry. Suspensions sampled in the reactor before CO₂ injection (t=0) and after CO₂ injection (t=2 and t=6 minutes).



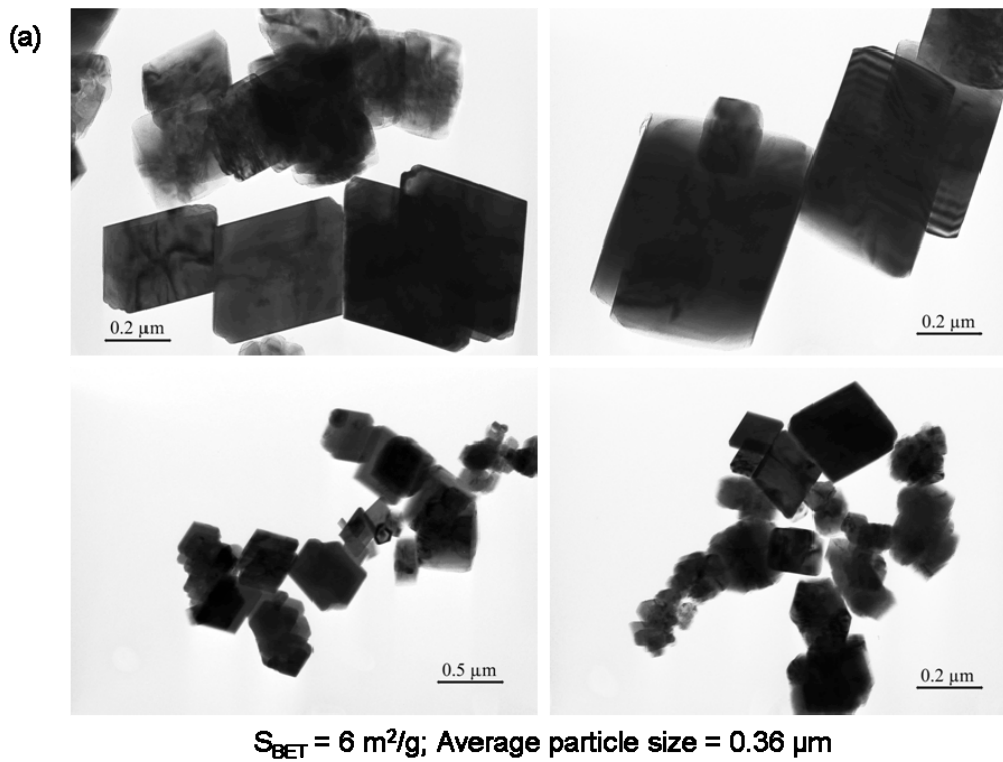
1

2



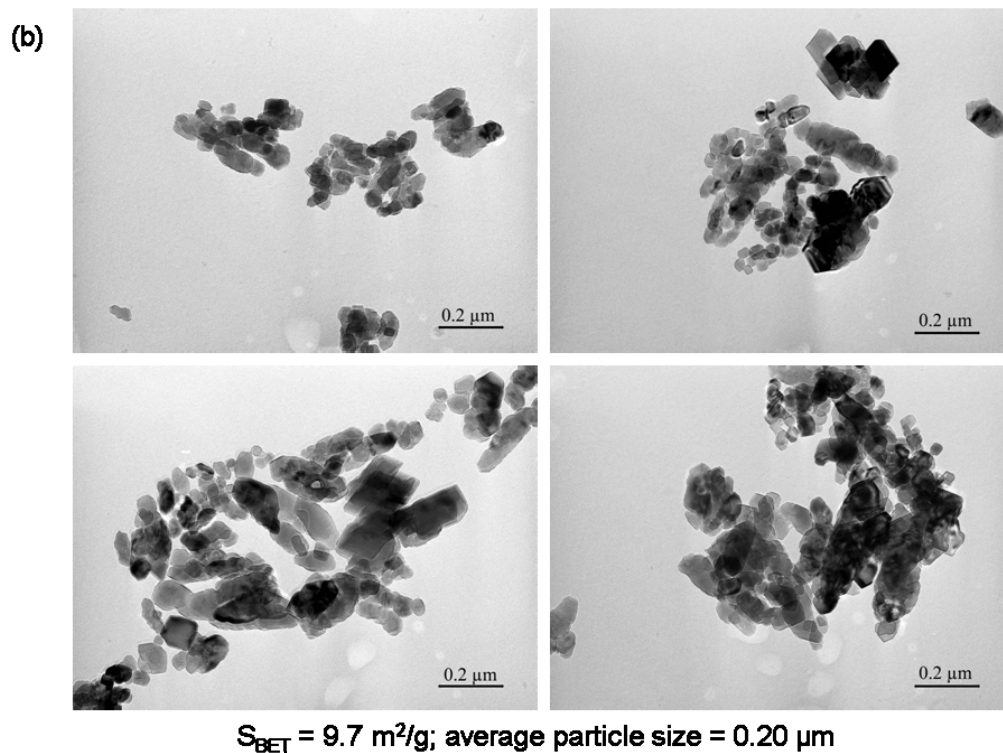
3

4 **Figure 3.** Ca-Concentration and pH behaviour with time for calcite precipitation at (a) 90 bar
 5 and 90 °C and, (b) 55 bar and 30 °C. Note that the pH and Ca-concentration measurements
 6 were carried out at 25 °C after filtration, cooling and degasification of the solutions



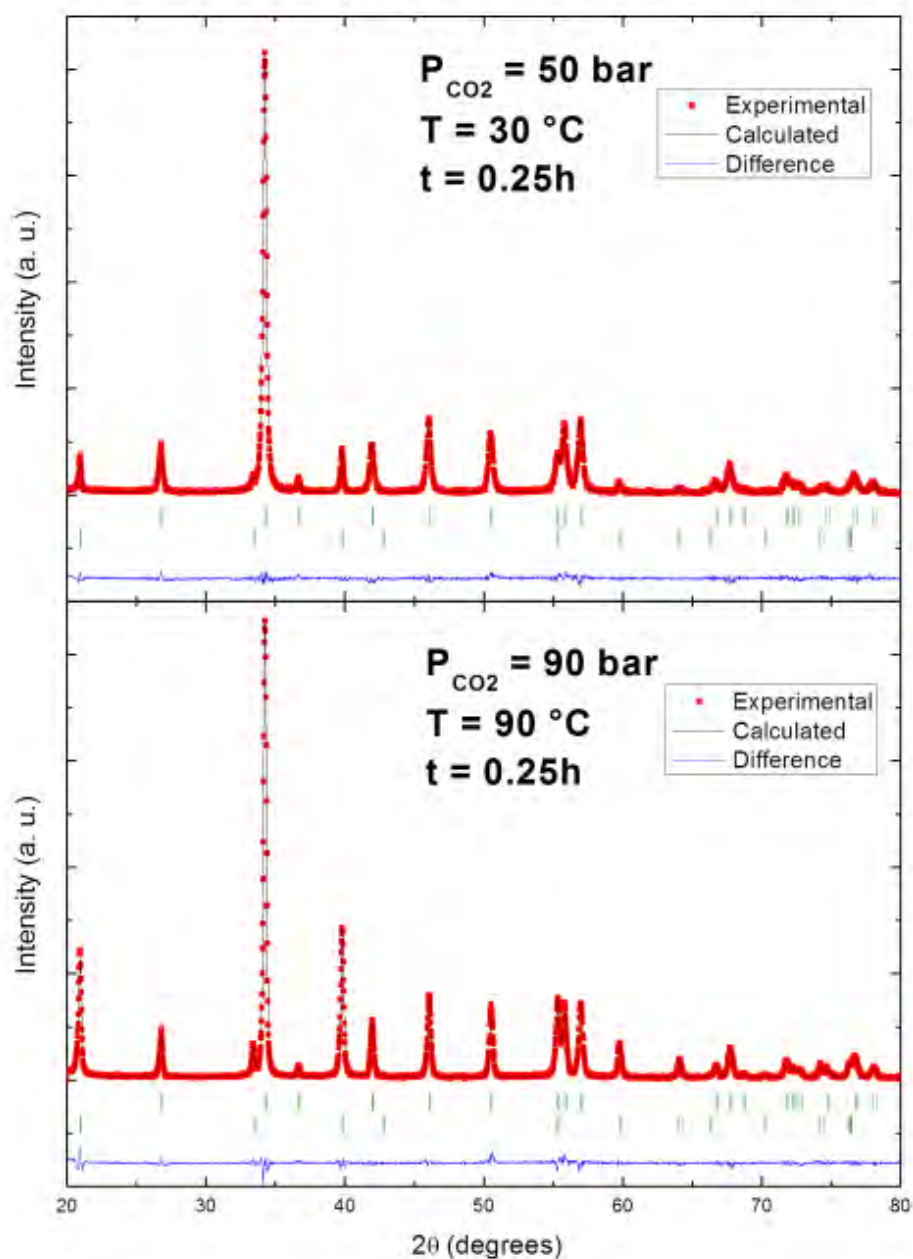
1

2



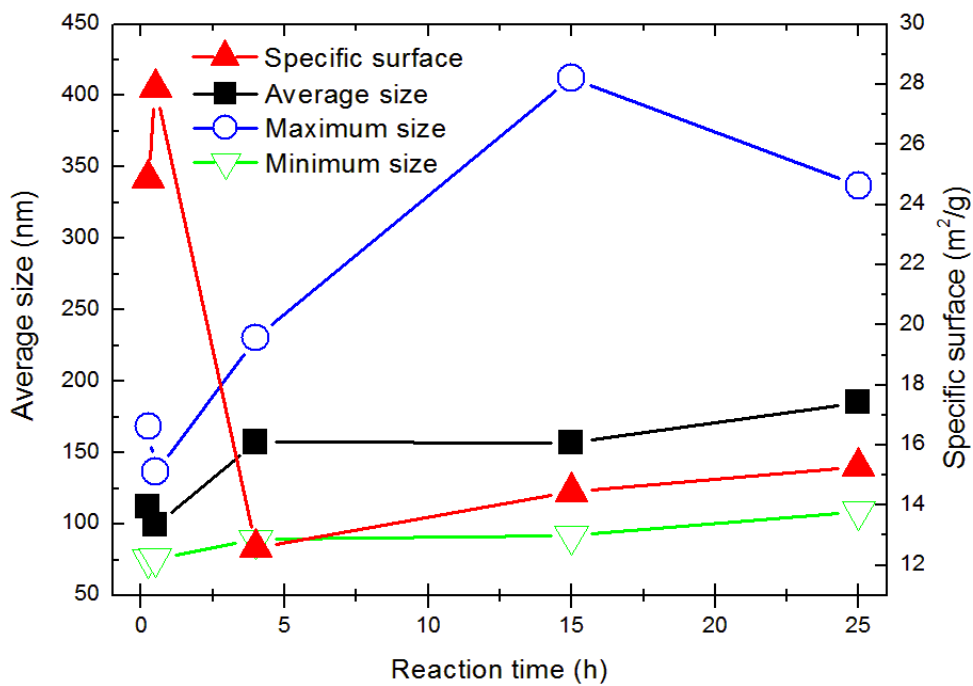
3

4 **Figure 4.** TEM micrographs showing the calcite particles precipitated from $\text{CO}_2\text{-H}_2\text{O-}$
 5 Ca(OH)_2 slurry in presence of (a) supercritical CO_2 “90 bar; 90 °C” and (b) gaseous
 6 CO_2 “55 bar, 30 °C” after 24h of reaction in batch system.



1
2
3
4
5
6
7
8

Figure 5. Experimental and Rietveld refined X-ray diffraction patterns for the calcite samples synthesized during 0.25 h. The green lines indicate the Bragg reflections. A secondary phase of Portlandite was introduced in all the refinements. An anisotropic spherical harmonics model for the particle size and an isotropic strain model were used to model the width of the Bragg reflections.



1
2
3
4
5
6
7
8
9
10
11

12 **Figure 6.** Evolution of the coherent domain average, maximum and minimum sizes and of the
13 specific surface area of the calcite samples obtained at 90 bar and 90°C.